Arabian Journal of Chemistry (2020) 13, 8080–8091

King Saud University

Arabian Journal of Chemistry

www.ksu.edu.sa
www.sciencedirect.com

ORIGINAL ARTICLE

Fe_3O_4-CuO-activated carbon composite as an efficient adsorbent for bromophenol blue dye removal from aqueous solutions

Ali Q. Alorabi [a,*], M. Shamshi Hassan [a,*], Mohamed Azizi [b,c]

[a] Chemistry Department, Faculty of Science, Albaha University, Albaha, P.O. Box: 1988, Saudi Arabia
[b] Faculty of Science and Arts-Qilwah, 65941, Albaha University, Saudi Arabia
[c] Laboratory of Natural Water Treatment, Water Research and Technologies Center (WRTC), BP 273, Soliman 8020, Tunisia

Received 18 July 2020; accepted 21 September 2020
Available online 1 October 2020

KEYWORDS

Fe_3O_4-CuO activated carbon composite;
Bromophenol blue;
Adsorption;
Thermodynamics;
Kinetics

Abstract Dye wastewater from industries is posing tremendous health hazards. The lethal dyes can be eliminated using nanomaterials and scientific approach like adsorption which is facile, cheap, safe as well as ecofriendly. Fe_3O_4-CuO-AC composite was prepared by a hydrothermal method and used for the removal of dyes in wastewater. The composite material was characterized by various techniques such as XRD, SEM, EDS, TEM and FT-IR. The Fe_3O_4-CuO-AC composite was used to treat five types of dyes in water. Fe_3O_4-CuO-AC composite showed the highest adsorption capability for bromophenol blue (BPB) dye. The effects of initial concentration, pH, the amount of adsorbent and temperature were also studied. The optimum conditions were found to be 20 ppm dye concentration, pH 9, an adsorbent dose of 0.06 gL^{-1} at 65 °C. A removal efficiency of 97% was obtained for BPB dye during 120 min of adsorption. Kinetic studies indicated that a pseudo-second order is the most suitable model for the adsorption process. The Fe_3O_4-CuO-AC composite showed better adsorption capacity as compare to Fe_3O_4-AC except for the Methyl green dye. The maximum adsorption capacity was found to be 88.60 mg/g for BPB. Additionally, the thermodynamic parameters ($\Delta S°$, $\Delta H°$ and $\Delta G°$) showed that the process was spontaneous and exothermic. All the above results revealed that the Fe_3O_4-CuO-AC compositecan be an effective adsorbent for removing dyes from wastewater.

1. Introduction

Paint, textile and pigment manufactories have been utilizing dyes widely for decades (Liu et al., 2011). Annually, about 1.6 million tons of dyes are being manufactured to fulfil projected industrial requirements. Approximately 10–15% of these dyes are being thrown away as wastewater (Hunger,

* Corresponding authors.
E-mail addresses: aalorabi@bu.edu.sa (A.Q. Alorabi), mshasan@bu.edu.sa (M. Shamshi Hassan).
Peer review under responsibility of King Saud University.

Production and hosting by Elsevier

https://doi.org/10.1016/j.arabjc.2020.09.039
1878-5352

2003). Consequently, overexposure to such dyes has resulted in potentially life threatening ailments such as skin and respiratory complications, as well as an increase inthe probability of human carcinoma (Lellis et al., 2019). Providing an environmental friendly and low-cost method to control and govern wastewater is thus a highly essential concern.

Among all the available dye wastewater treatment techniques (Wang, 2020; Naghan, 2015), adsorption is a prominent approach due to its effectiveness, economy and simplicity (Wang et al., 2019; Wu et al., 2019; Karami et al., 2017). Designing an efficient adsorbent for removing colored dyes for wastewater treatment is a challenge. Carbon nanomaterials and graphene oxide have attracted much interest for various applications (Wang et al., 2020; Wang et al., 2015; Xu, 2020; Azari, 2017). Activated carbon (AC) is frequently used as adsorbent, it features a porous structure and thus has huge specific surface area and strong adsorption capacity. As such it is widely used for the removal of organic dyes and pollutants from industrial wastewater (Daoud et al., 2019; Senthil Kumar et al., 2018; Zhang et al., 2018). AC can remove many dyes but its adsorption efficiency is low (Abdullah et al., 2009). To overcome these disadvantages, composites of AC with metal oxide nanoparticles can be a good option.

Metal oxide nanomaterials are drawing attention as a suitable alternative for the treatment of wastewater (Liu et al., 2019; Shaheen, 2020; Gautam et al., 2020; Li et al., 2020; Azari, 2014). However, metal oxides are likely to agglomerate due to van der Waals forces or additional interactions (Sousa and Teixeira, 2020) which lead to a decrease in capacity and selectivity. To advance the applicability of nanomaterial oxides in wastewater treatment, they have been mixed with porous matrix of AC. Recently, magnetic adsorbents have gained immense attention for water treatment, owing to their ease of separation and collection by a magnet. Simultaneously, mixing with magnetite particles can reduce agglomeration of particles. Liu et al. (2011) have reported on Fe_3O_4/GO composite that featured higher adsorption compared to Fe_3O_4. Meanwhile, the low cost, easy synthesis and superparamagnetic properties make these affordable and reusable materials. The lowcost copper-based metal oxides (CuO) are also gaining large interest becauseof their potential towards diversified applications. Adsorption properties of copper and CuO as adsorbent for degradation of different dyes have been reported ealier (Shu et al., 2017; Dashamiri et al., 2016). CuO nanoparticles have tendency to bind on AC surface through Cu and oxygen reactive center. Morover, its incorporation with AC has greatly inhanced AC-based adsorbent efficiency forthe removal of water contaminats (Dashamiri et al., 2016; Peternela et al., 2018). Therefore, synthesis of novel metal oxides hybrid adsorbents can be an effective method to overcome all aforementioned technical problems.

The aim of the present work wasto prepare Fe_3O_4-AC and Fe_3O_4-CuO-AC composite adsorbents using cost-effective and nontoxic metal precursorsby a simple hydrothermal methodand apply these for removing dyes in wastewater. The adsorption properties of the materials towards five different dyes were investigated under different experimental parameters such as adsorbent dosage, contact time, pH and temperature. The novel composite shows the high adsorption efficiency against wide range of frequently used toxic industrial dyes.

2. Experimental method

2.1. Materials required

Commercial AC was purchased from BDH Company (BDH Chemicals Ltd., Pool, UK). Iron (III) chloride ($FeCl_3{\cdot}6H_2O$; 97%), Iron (II) chloride ($FeCl_2{\cdot}6H_2O$), ammonium solution (25%), copper acetate powder, sodium hydroxide (NaOH) were of analytical grade, purchased from Sigma-Aldrich, Dorset, UK. Fuchsin acid (FA), methyl green (MG), murexide (MX), methyl orange (MO), and bromophenol blue (BPB) with respective molecular formula of $C_{20}H_{17}N_3Na_2O_9S_3$, $C_{27}H_{35}BrClN_3{\cdot}ZnCl_2$, $C_8H_8N_6O_6$, $C_{14}H_{14}N_3NaO_3S$ and $C_{19}H_{10}Br_4O_5S$ molecular weights of 585.53, 653.24, 284.188, 327.33, 669.96 $gmol^{-1}$ were obtained from Lobe Chemie, India.

2.2. Preparation of Fe_3O_4 nanoparticles loaded on activated carbon

0.9 g of AC was added to 80 mL of aqueous salts solution of $FeCl_3{\cdot}6H_2O$ (1.62 g) and $FeCl_2{\cdot}6H_2O$ (0.63 g) and the final solution was stirred to load the ions on the AC (Salari et al., 2019; Moazzen et al., 2019). Then, 2 M of NaOH solution was added dropwise to the solution under vigorous stirring until the solution reached pH 10–11 at room temperature (25 °C). The mixture was transferred to a Teflon-lined stainless steel autoclave which was heated at 200 °C for 12 h. After cooling at room temperature (25 °C), the solution was filtered and the precipitate washed several times with deionized water and then with ethanol. Finally, the sample was dried in an oven at 80 °C for 12 h.

2.3. Preparation of Fe_3O_4-CuO nanoparticles loaded on activated carbon

First the magnetic nanoparticles were synthesised using the hydrothermal method as reported by Ahmadi et al. (2012) with some modifications. Briefly, $FeCl_3{\cdot}6H_2O$ (1.62 g) and $FeCl_2{\cdot}6H_2O$ (0.63 g) were dissolved in 80 mL of deionized water. The solution was stirred and ammonium solution (25%) was added quickly. The mixture was then transferred to the hydrothermal reactor and heated at 200 °C for 12 h. Subsequently, the mixture with the formed magnetic nanoparticles was cooled to room temperature, filtered and washed several times with deionized water, and ethanol and finally dried in an oven at 80 °C for 12 h.

Further, 0.3 g of the synthesized Fe_3O_4nanoparticles and 0.9 g of AC were added into 60 mL of distilled water in a beaker and sonicated for 10 min. Copper acetate (0.9 g) was dissolved in the same solution while stirring. A 2 M NaOH solution was added until precipitation occurred at pH ~ 10–11. Then the final solution was transferred to the hydrothermal autoclave and heated at 200 °C for 5 h. Later, the precipitate was filtered and washed several times with deionized water and ethanol. The powdered sample was dried in an oven at 80 °C for 12 h and ground with mortar and pestle to a fine powder.

2.4. Characterization of Fe_3O_4-AC and Fe_3O_4-CuO-AC composites

Scanning electron microscopy (SEM) coupled with energy-dipersive X-ray (EDX) (SEM, Philips XL30ESEM-TMP) analysis was used to observe the surface morphology and surface texture of the materials and to determine the elemental content in composite samples. An X-ray diffraction (XRD) system (Philips PW1825) was used to confirm the crystalline stuructures of the composite samples. Fourier transform infrared spectroscopy (FTIR, Thermo Scientific ATR) was performed in the transmittance mode, in the range of 400–4000 cm^{-1}. The microscopic features of composite sample was examined under transmission electron microscope (TEM) (H-7650, Hitachi, Japan). The thermal stability of the sample was characterized by thermogravimetric analysis (TGA-DTA, Perkin–Elmer Inc., USA) under air with a flow rate of 20 mL/min. The samples (~2–5 mg) were heated in a platinum pan from an ambient temperature to 1000 °C in air environment. Initial weight of the sample taken was 15 mg and calcined at scan rate of 20 °Cmin^{-1}.

2.5. Adsorption experiments

Five different dyes (MX, MO, MG, FA and BPB) were chosen to test the adsorption efficiency of the single and bimetallic AC composites. In these experiments, the concentration of all five dyeswas 20 mgL^{-1}, and the pH values were: MX (pH 4–5), MO (pH 5–6), MG (pH 4–5), FA (pH 4–5) and BPB (pH 5–6). In atypical experiment, 40 mg of adsorbent materials were dispersed into 100 mL of each of the five dye solutions with stirring. From the adsorption performance resultsof Fe_3O_4-CuO-AC composites, the BPB dye was chosen to further study the effect of parameters on adsorption including the initial dye concentration, time, adsorbent dosage and temperature. To study the effect of time and initial dye concentration on adsorption, a fixed amount of the adsorbent (0.1 g) was added into 250 mL of aqueous BPB dye solution with varying concentration from 10 mgL^{-1} to 40 mgL^{-1} and mixed for different times ranging from 15 to 120 min at room temperature.

Effect of adsorbent dosage on adsorption: Different amounts (20, 40,60,80,100 mg) of adsorbentwere mixed with 100 mL of BPB (20 mgL^{-1}) for 2 h at room temperature.

Effect of temperature on the adsorption: 0.1 g of adsorbent was mixed with 200 mL of BPB dye (20 mgL^{-1}) at different temperatures (15 °C, 45 °C and 65 °C).

Effect of pH of BPB dyeon adsorption: 0.1 g of adsorbent was mixed with 100 mL of BPB dye solution (20 mgL^{-1}) for 2 and 24 h at different pH solution (3, 5, 7, 9 and 11) and at room temperature.

In all batch adsorption experiments, about 3 mL of supernatant was taken, centrifuged at 5000 rpm for 5 min, and the residual dye concentration analysed via UV/vis spectrophotometer (Thermo Fisher Scientific Evolution 300 UV–visible double beam spectrophotometer (USA).

Theadsorption capacity of the adsorbent, Q_e (mg/g) and the removal efficiency (R) were calculated at the equilibrium conditionsfrom the following equation:

$$R\% = \left(\frac{C_0 - C_e}{C_0}\right) \times 100 \quad (1)$$

$$Q_e = \frac{(C_0 - C_e)V}{M} \quad (2)$$

where C_o and C_e are the initial and equilibrium concentrations (mg/L) of BPB dye, respectively, V is the volume (L) of the metal solution, and M is the mass of adsorbent used (g). Kinetic models were investigated to understand the adsorption dynamics of BPB on the Fe_3O_4-CuO-AC composites. The linear form of Lagergren first-order rate equation is:

$$\log(Q_e - Q_t) = \log(Q_e) - \frac{K_{1ad}}{2.303}t \quad (3)$$

where Q_e and Q_t (mg/g) are the adsorption capacity at equilibrium and after time t (min), and k_{1ad} is the first-order rate constant (min^{-1}), respectively.

The linear form of second-order rate equation is:

$$\frac{t}{Q_t} = \frac{1}{k_{2ad}Q_e^2} + \frac{1}{Q_e}t \quad (4)$$

where k_{2ad} is the pseudo-second order equilibrium constant ($g{\cdot}mg^{-1}{\cdot}min^{-1}$).

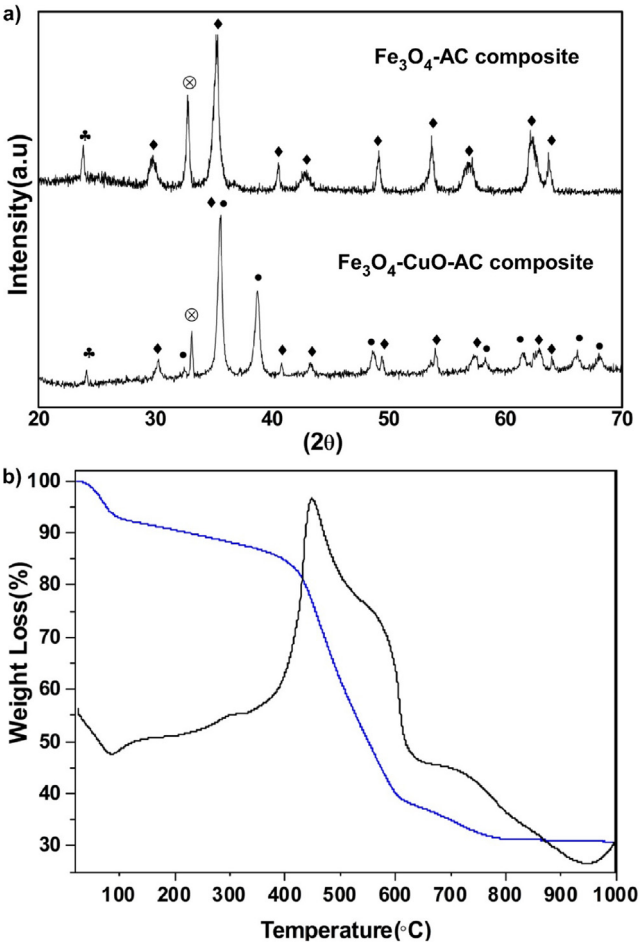

Fig. 1 (a) XRD spectra of (down) Fe_3O_4-CuO-AC sample and (Top) Fe_3O_4-AC-composite, (b) The TGA (blue line) and the DTA (black line) analysis of Fe_3O_4-CuO-AC composite.

3. Results and discussion

3.1. Characterization of adsorbent

The XRD spectra (Fig. 1a) for both the Fe_3O_4-AC and Fe_3O_4-CuO-AC samples indicated the presence of a peak at ~25°revealing the presence of amorphous carbon (Gao et al., 2013). For the Fe_3O_4-AC sample, the spectrum showed the peaks indexed as planes (220), (311), (400), (422), (511) and (440) corresponding to thecharacteristic of a cubic spinel structure of Fe_3O_4. The Fe_3O_4-CuO-ACcomposite showed additional peaks to those of the AC and Fe_3O_4. These additional peaks showed the diffraction pattern of CuO. The position of all the diffraction peaks matched well with the reported literature (JCPDS file No. 05-661) (Hassan, 2012). The peak marked with the symbol (*) indicated an impurity, a crystalline phase associated to sodium in both spectra. The thermal stability of the Fe_3O_4-CuO-AC composite was examined via TGA-DTA and the results are shown in Fig. 1b. The first thermal weight loss between 25 and 150 °C was around 9%. This maybe due to the dehydration of residual water molecules from the sample surface which was accompanied by a small endothermic peak in the DTA curve. A small weight loss (4.5%) was noticed in the range of 150–380 °C because of the decomposition of the metal precursor functional group and volatile organic material. The major weight loss of 62% occurred between 400 and 800 °C due to the degradation of carbon molecules. This weight loss appeared with a strong exothermic peak (450 °C) in the DTA curve.

Fig. 2(a, b) show the morphology of the sample which were observed by SEM. CuO-Fe_3O_4-AC composite exhibited a flake-like structure with a homogeneous distribution of CuO and Fe_3O_4 oxide nanoparticles all over the surface of the AC. This was also confirmed from TEM images of Fe_3O_4-CuO-AC sample (Fig. 2c). The dark and lighter color nanoparticles seem to be of Fe_3O_4 and CuO on the AC surface. The average size of both these particles appears to be less than 100 nm. Therefore, it can be concluded that the metal oxides were successfully loaded on the surface of AC. The elemental compositions of Fe_3O_4-AC and Fe_3O_4-CuO-AC composites were determined from EDX spectra are shown in Fig. 3a, b. The presence of Fe, Cu, O and C in the composite confirms the formation of Fe_3O_4-CuO-AC. Additionally, the atomic ratio of Fe, Cu and C is approximately 1 for the composite (Fig. 3a).

3.2. Adsorption experiment

The adsorption performance of Fe_3O_4-AC and Fe_3O_4-CuO-AC composite for the five dyes was investigated and is

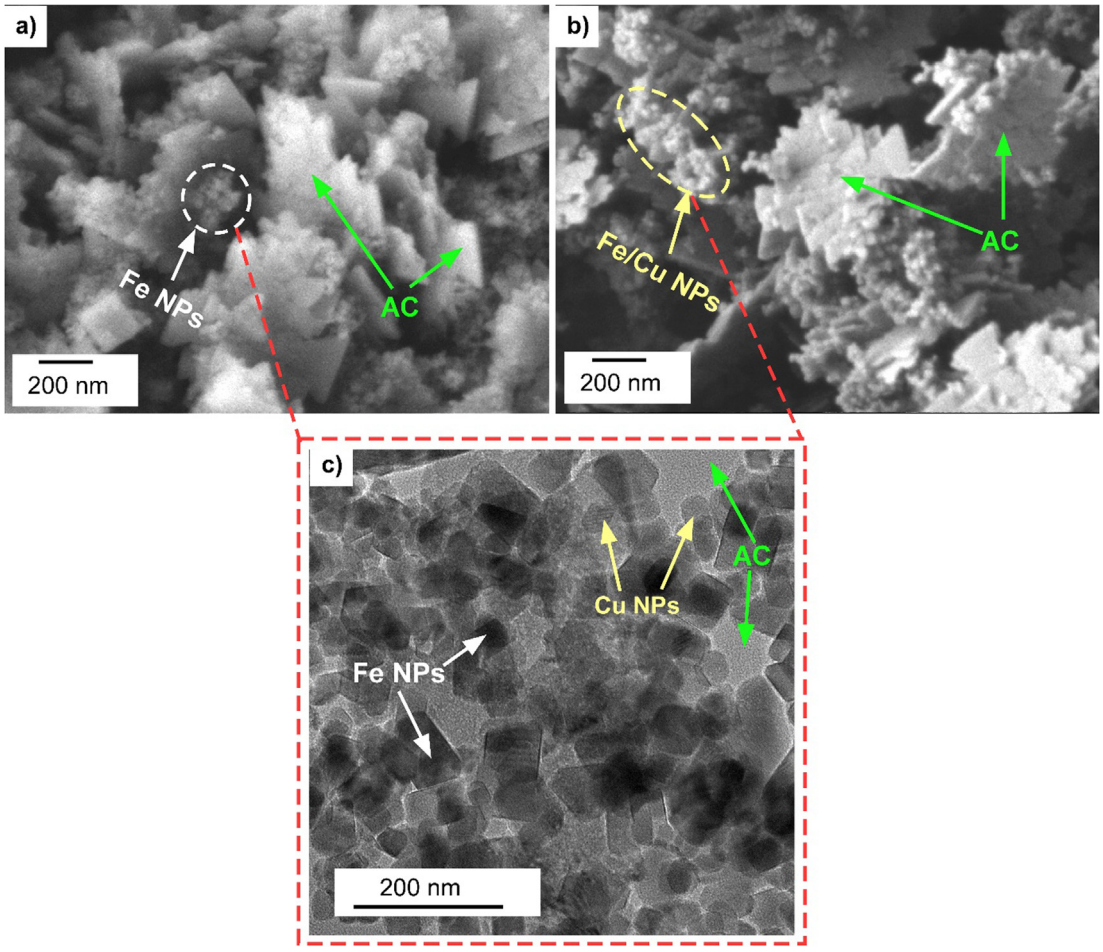

Fig. 2 (a, b) SEM images and (c) TEM image of Fe_3O_4-CuO-AC composite.

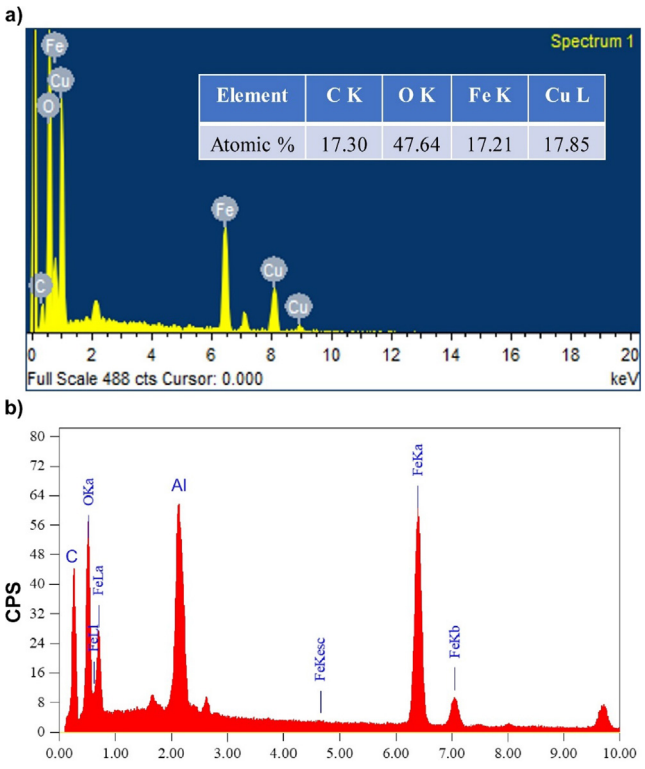

Fig. 3 EDX spectra of (a) Fe_3O_4-CuO-AC and (b) Fe_3O_4 -AC composite.

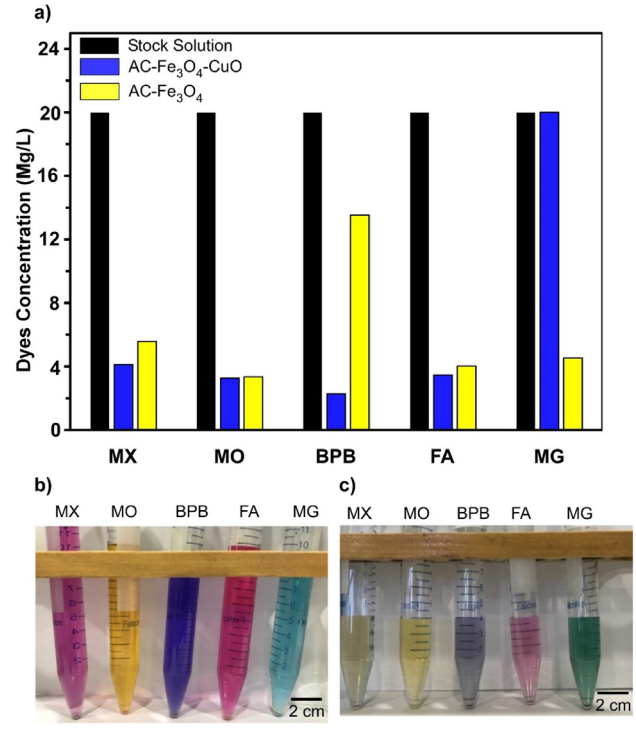

Fig. 4 (a) The adsorption performance of Fe_3O_4-CuO-AC composite (yellow bar) and Fe_3O_4-AC (blue bar) after 2 h for the five dyes. Image of dye adsorption (b) before and (c) after 2 h.

summarized in Fig. 4. As shown in the bar chart (Fig. 4a), after 2 h, the adsorption capacity of the Fe_3O_4-CuO-ACcomposite for MX, MO, MG, FA and BPB dyes was superior to that of the Fe_3O_4-AC composite. Whereas, in case of MG dye, the Fe_3O_4-AC composite showed much better adsorption, while the Fe_3O_4-CuO-AC composite did not show any noticeable adsorption. The Fe_3O_4-CuO-AC composite showed the lowest concentration of BPB dye (2.3 mg/L) after 2 h (Fig. 4a). This indicates the high adsorption capability of Fe_3O_4-CuO-AC composite especially for BPB dye. Fig. 4(b and c) show the images before and after adsorption of dyes with Fe_3O_4-CuO-AC composite. The mechanism for the high adsorption capacity for BPB dye is that at pH < 7, under acidic medium negatively charged BPB blue dye results in positive charged surface of AC-Fe_3O_4-CuO composite. Therefore, negative BPB dye favouring bonds with Fe^{3+} and Cu^{2+} due to the electrostatic attraction. Also, the π–π physical interaction play an important role in the adsorption mechanism, that is built up between the aromatic structures of both the dye and the activated carbon (Shu et al., 2017). Moreover, the higher adsorption activity Fe_3O_4-CuO-AC composite maybe ascribed to the synergistic effect of Fe_3O_4 and CuO on activated carbon surface.

Fig. 5 showed the FT-IR spectra of Fe_3O_4-CuO nanoparticles loaded activated carbon before and after treatment with BPB dye. It displayed two conjoint peaks at 566 and 610 cm^{-1} assigned to tetrahedral Cu/Fe ions-oxygen vibrations (Khan et al., 2015), confirming the presence of Cu and Fe species over activated carbon surface. The peaks at 1390 and 1510 cm^{-1} were attributed to symmetric carboxylate groups and C═O (aliphatic ketone) stretch of acetone. The peaks at 3290, 3330, and 3450 cm^{-1} were associated with ─OH stretching vibrations. After BPB adsorption over Fe_3O_4-CuO nanoparticles loaded activated carbon shifting and change in intensities of peaks was observed. A slight shift along with change in intensities of conjoint peaks at 566 and 610 cm^{-1} to 557 and 591 cm^{-1} was observed depicting their involvement in anionic BPB adsorption due to electrostatic forces. Reductions in peaks size at 1390 and 1510 cm^{-1} affirmed their involvement during BPB adsorption. This also suggest the stability of the composite material after treatment with dye.

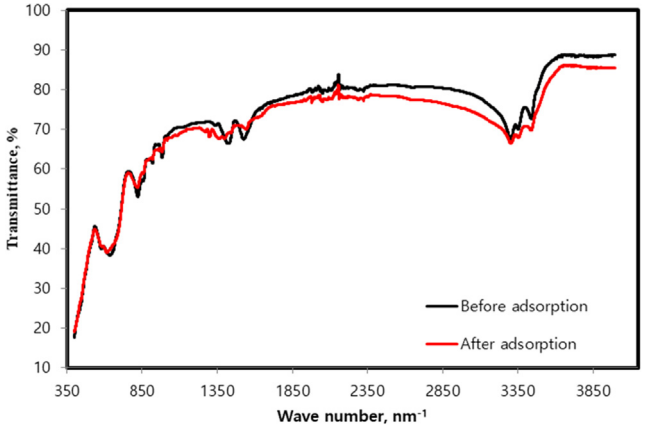

Fig. 5 FT-IR spectra of Fe_3O_4-CuO-AC composite before and after treatment with BPB dye.

3.3. Effect of time, concentration and temperature

The effect of contact time on BPB dye removal at different initial concentrations (10–40 mgL^{-1}) is represented in Fig. 6a. These data were recorded at a constant pH of 5.3, adsorbent dosage 0.1 g and a temperature of 25 °C. Adsorption was found to increase with increasing contact time at all initial dye concentrations and equilibrium was attained within about 30 min. At the beginning the adsorption capacity was high due to the abundant availability of active sites for dye adsorption. Following this, the rate of dye uptake became virtually insignificant, probably due to electrostatic repulsion between the negatively charged adsorbate onto the surface and the available anionic sorbate species in solution. Additionally due to the slow pore diffusion of the BPB into the bulk of the adsorbent, the rate of adsorption did not change significantly (Ghaedi et al., 2012; Xiang, 2019). Furthermore, the amount of BPB dye uptake, q_t (mg/g) increased with increasing adsorbate concentration. This was because the increase in initial dye concentration also increased the interaction between dye and adsorbent, thereby causing higher dye uptake (Malkoc, 2006; You et al., 2006).

The removal of BPB dye as a function of temperature (from 15 to 65 °C) was also examined under acondition of 0.1 g sorbent mass at pH 5.3 (Fig. 6b). The adsorption capacity slightlyincreased with increase in temperature, showing an endothermicnature of the sorption reaction. This may be due to the rapid rate of diffusion of molecules at high temperature. The result is consistent with results reported for methylene blue adsorption on AC-CuO (Shu et al., 2017), BPB adsorption on polymer-clay composite (El-Zahhar et al., 2014) and Congo Red (CR) dye removal by iron particles (Kim and Choi, 2017).

3.4. Effect of adsorbent dosage

The effect of the adsorbent dosage on the removal efficiency of BPB dye was studied by adding different amounts of Fe_3O_4-CuO-AC composite (0.02, 0.04, 0.06, 0.2, 0.08, and 0.1 g) at a constant dye concentration (Fig. 7a). The removal

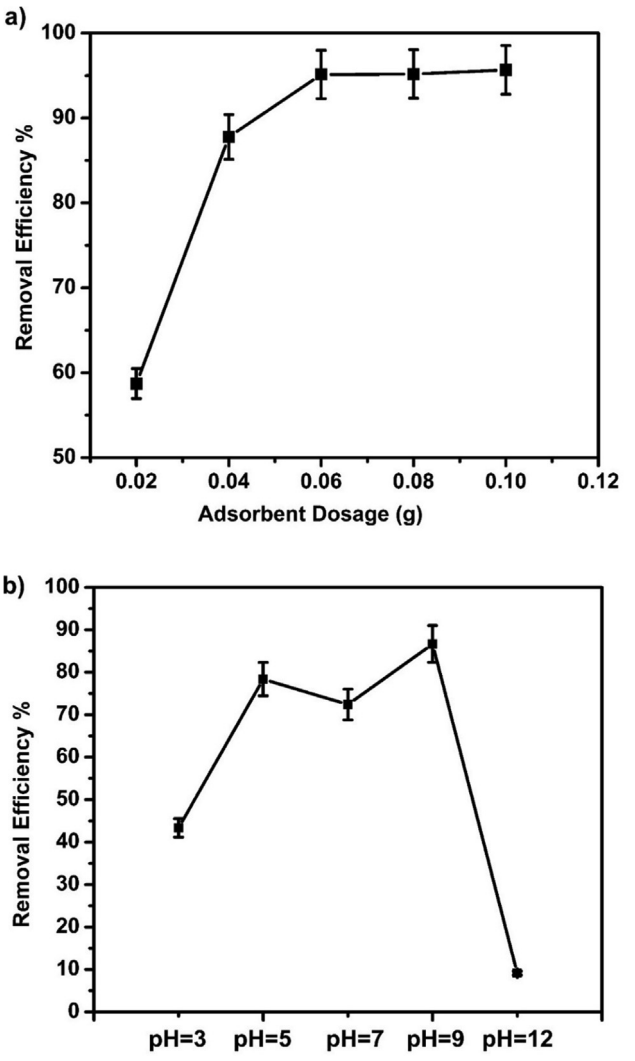

Fig. 7 (a) Effect of adsorbent amount on removal of dye (pH = 5–6, Ci = 20 mg/L, Temp. = 25 °C, time = 120 min). (b) Effect of the medium pH on removal of dye (Ci = 20 mg L^{-1}, temp. = 25 °C, adsorbent dose = 0.1 g, time = 120 min.)

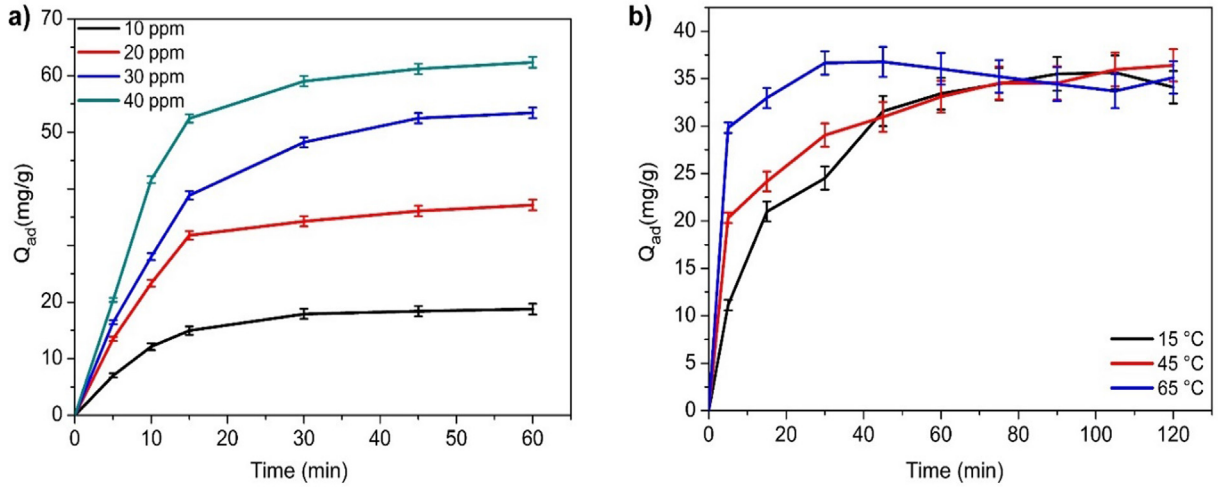

Fig. 6 (a) Effect of the time and initial concentration of BPB dye on sorption (b) Effect of the temperature on removal of BPB dye (pH = 5.3, Ci = 20 mg L^{-1}, adsorbent dose = 0.1 g).

efficiency of BPB dye increased from 58% to 95% with increasing Fe_3O_4-CuO-ACdosage from 0.02 to 0.06 g. The initial rapid increase of adsorption with increasing adsorbent dosage is attributed to the availability of more adsorption sites. However, with a further increase in Fe_3O_4-CuO-AC dosage beyond 0.06 g, as more dye molecules adsorbed on the composite surface thus resulted in fewer available sites (Zheng et al., 2018; Cao et al., 2017; Okoye, 2018).

3.5. Effect of pH on dye adsorption

The pH value plays an important role in aqueous chemistry and the surface binding sites of the adsorbents. The influence of the pH on BB removal by the Fe_3O_4-CuO-AC composite was studied in the range from pH 2 to 12 (Fig. 7b). The results showed that an increase from pH 3 to 9 caused an increase in dye removal efficiency. A decrease was observed when the pH value was above 9. At low pH, the dye molecule exists as a negative ion in solution which interacts with the positively charged adsorption sites, enhancing adsorption through electrostatic attraction. At high pH values, with the increase in HO^-ion concentration, competition increases with cationic adsorption sites resulting in the decrease in removal efficiency (Dashamiri et al., 2016; You et al., 2006; Okoye, 2018; Tabassum, 2015).

3.6. Adsorption kinetics

The study of adsorption kinetics is an important aspect for understanding the reaction mechanism for dye adsorption. To investigate adsorption kinetics of BPB on adsorbents, pseudo-first order (Lagergren, 1898; Ghaedi et al., 2014) and pseudo-second-order models (Ho, 2006; Mazaheri et al., 2016) were selected to fit experimental data (Fig. 8). The parameter data of the two models were calculated and are summarized in Table1. The adsorption rate can be predicted which provides information for the design and model the process. Fig. 8 shows straight-lineplots of $\ln(Q_e - Q_t)$ versus t and t/Q_t versus t, respectively, which were drawn to determine the values of k_1, k_2 and correlation coefficients (R^2). For different initial concentrations and temperatures, the correlation coefficients (R^2) of the pseudo-second-order model is more suitable to describe the adsorption kinetic data than the pseudo-first-order model. This can be confirmed by comparing the calculated $Q_{ad,}$ value with the experimental one. For example, at higher temperature (especially at 65 °C), the calculated adsorption amount at equilibrium agrees reasonably well with the experimental data in the pseudo-second-order model (38.461≈36,766 (mg/g) >> 07.533 (mg/g) than the pseudo-first-order model). Also, it is noted that the values of k_2

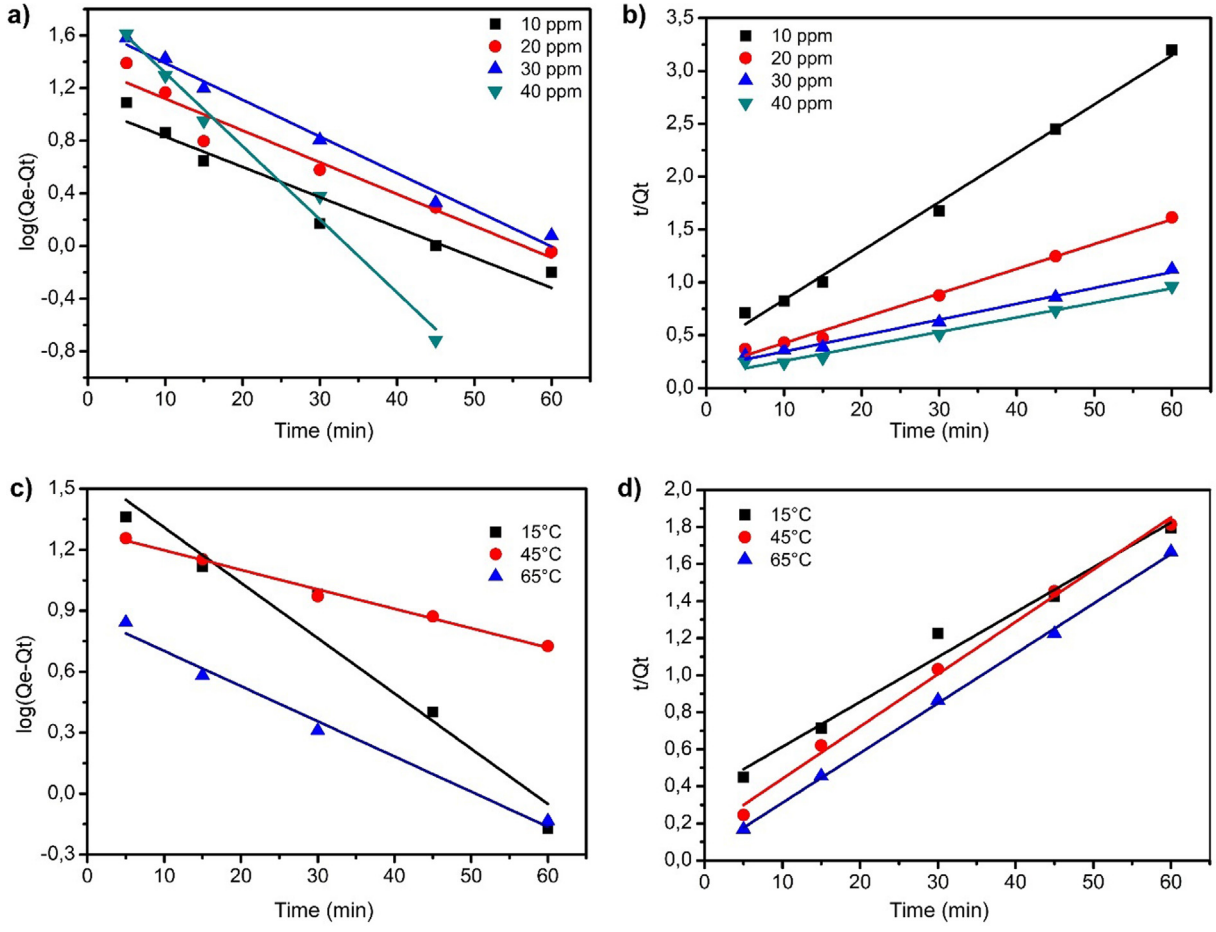

Fig. 8 Plots of pseudo-first-order and pseudo-second-order kinetic model for adsorption of BPB onto activated carbon-Fe_3O_4-CuO composite; (a, b) effect of the initial concentration and (c, d) effect of the temperature.

Table 1 Kinetic parameters for the pseudo-first and pseudo-second-order adsorption model.

C_o (mg/l)	$Q_{ad,exp}$ (mg/g)	First-order			Second-order		
		$k_1(min^{-1})$	R^2	$Q_{ad,theo}$(mg/g)	$k_2(g{\cdot}mg^{-1}{\cdot}min^{-1})$	R^2	$Q_{ad,theo}$(mg/g)
10	19,387	0.0529	0.937	11,508	5.68×10^{-3}	0.995	21.739
20	38,055	0,0552	0.950	23.014	2.78×10^{-3}	0.992	43.478
30	54,608	0,0621	0.988	46.665	1.15×10^{-3}	0.992	66.666
40	61,389	0,1266	0.986	74.644	1.43×10^{-3}	0.986	76.923
Temperature (°C)							
15	34,090	0,0621	0.952	38.106	1.55×10^{-3}	0.982	41.666
45	38,402	0,0207	0.991	19.588	4.96×10^{-3}	0.995	35.714
65	36,766	0,0414	0.979	07.533	16.09×10^{-3}	0.999	38.461

*$Q_{ad,theo}$ is the theoretical adsorption capacity and $Q_{ad,exp}$ is the experimental adsorption capacity.

increased from 1.55×10^{-3} ($g{\cdot}mg^{-1}{\cdot}min^{-1}$) at 15 °C compared to 16.09×10^{-3} ($g{\cdot}mg^{-1}{\cdot}min^{-1}$) at 65 °C. An increase in adsorption reaction temperature was accompanied by a decrease of $Q_{ad,theo}$ values. This indicates the endothermic nature of BPB adsorption reaction on the Fe_3O_4-CuO-AC composite (Ghosh, 2019).

The second-order rate constants (K_2) listed in Table 1 were used to estimate the adsorption activation energy (E_a) using the Arrhenius equation (You et al., 2006).

$$\ln k = \ln A - E_a/RT \quad (5)$$

The slope of ln k vs $1/T$ was used to determine E_a, which was found to be $E_a = 2.583$ kJ mol^{-1}. The activation energy barrier of this adsorption reaction is sufficiently small to be provided readily from mechanical agitation of the reaction mixture at room temperature for transfer of BPB species from solution over the surface of the composite for adsorption (Ghosh, 2019).

The experimental results showed that the adsorption equilibrium was reached within the long time (especially when we studied the effect of temperature). Firstly, it has been suggested that the Fe_3O_4-CuO-AC composite is a porous adsorbent (You et al., 2006; Zhao et al., 1989). Secondly, the internal diffusion (or intraparticle diffusion), are stages of the adsorption process. The most widely applied intraparticle diffusion equation for adsorption system is given by Weber and Morris (Bhattacharyya and Sharma, 2004).

$$Q_{ad} = k_{id} \cdot t^{1/2} \quad (6)$$

The linear relationship between Q_{ad} and $t^{1/2}$ is shown in Fig. 9 suggesting that internal diffusion limits the adsorption process. That can be explained by the increase of temperature. High temperature accelerates external and internal diffusion. Changing temperature will change the equilibrium adsorption capacity. The presence of a linear section is clearly observed for BPB adsorption (Fig. 9). This indicates that the adsorption mechanism in this case is controlled by two steps. The first step is related to mass transfer to the outer surface of the Fe_3O_4-CuO-AC activated carbon composite while the second step is for intraparticle diffusion (internal diffusion). The rate constants of intraparticle diffusion k_{id} ($g{\cdot}mg^{-1}{\cdot}min^{-1/2}$) are listed in Table 2.

The intraparticle diffusion energy $E_{id} = 16.494$ kJ $mol^{-1}$was determined from the slope of $\ln k_{id}$ (rate constant listed in Table 2) vs $1/T$. The energy of adsorption was less than 25–30 kJ mol^{-1}. Due to the rates of reaction, sorption increased more rapidly than those of diffusion processes with temperature.

3.7. Adsorption thermodynamics

To estimate the feasibility of the adsorption process, thermodynamic parameters, such as Gibbs free energy change (ΔG^o), enthalpy change (ΔH^o) and entropy change (ΔS^o) can be determined by applying the following equations (Bhatnagar, 2007; Mohammadzadeh et al., 2016):

$$\Delta G^0 = -RT\ln K \quad (7)$$

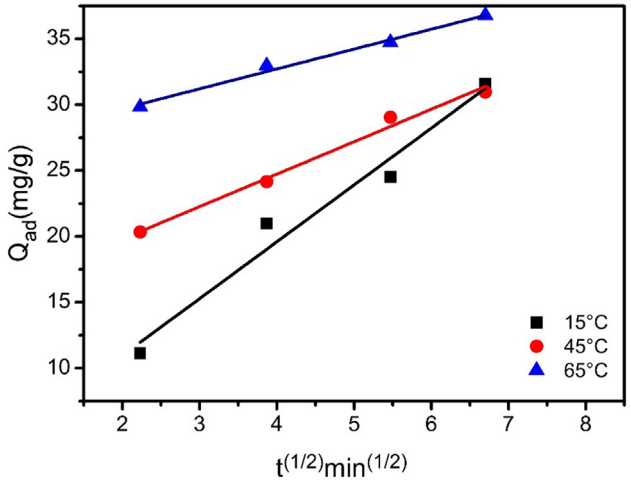

Fig. 9 Plots of adsorption capacity (Q_{ad}) vs $t^{1/2.}$

Table 2 Rate constant of intraparticle diffusion for Bromophenol Blue adsorption.

Temperature (°C)	k_{id} ($g{\cdot}mg^{-1}$ $min^{-0.5}$)
15	1.508
45	2.462
65	4.313

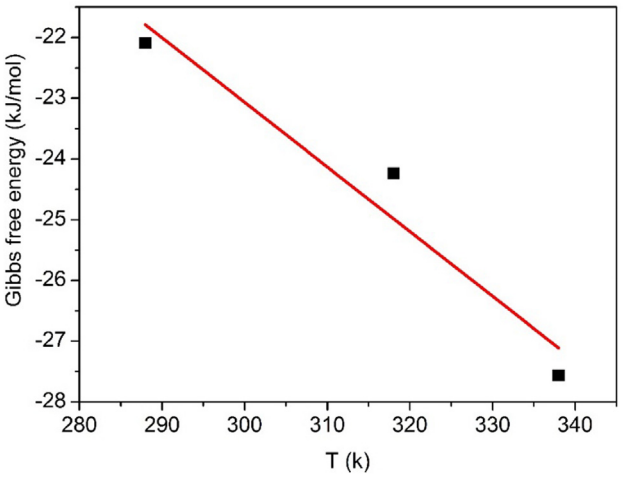

Fig. 10 Van't Hoff plot of BPB dye adsorption onto Fe_3O_4-CuO-AC composite.

Table 3 Thermodynamic parameters for adsorption of BPB on Fe_3O_4-CuO-AC composite.

Temperature (K)	ΔG^o (kJmol^{-1})	ΔH^o (kJmol^{-1})	ΔS^o (Jmol^{-1} K^{-1})
288	−22,093	8865	0,106
318	−24,240		
338	−27,566		

$$\Delta G^0 = \Delta H^0 - T\Delta S^0 \quad (8)$$

where K, R and T is the equilibrium constant, the gas constant (8.314 J·mol^{-1}·K^{-1}) and the absolute temperature (K), respectively. ΔH^o and ΔS^o were calculated from the slope and the intercept of the plots of ΔG^o versus T (Fig. 10). All thermodynamic parameters at all temperatures are reported in Table 3.

The values of ΔH^o and ΔS^o are assumed to be temperature-independent and can be considered as virtually constant. The negative value of ΔG^o indicates that the adsorption of BPB on the Fe_3O_4-CuO-AC compositeis a spontaneous process (El-Gamal et al., 2015). The adsorption process was more favorable at higher temperatures (El-Gamal et al., 2015). This phenomenon indicates the affinity of BPB on the Fe_3O_4-CuO-AC composite increases with increasing temperature which leads to the decreasing of corresponding Gibbs free energy value. The positive value of the enthalpy of adsorption (ΔH^o) shows that the adsorption process is endothermic for both samples, involves chemisorption reaction. So, raising temperature leads to increased adsorption of BPB at equilibrium.

3.8. Recycling of Fe_3O_4-CuO-AC composite

The AC-Fe_3O_4-CuO composite was reused for adsorptions–desorption cycle of BPB dye. The adsorption efficiency of Fe_3O_4-CuO-AC composite was checked for three cycle. In first cycle the adsorption was (91.90%), in second cycle, it was 88.27%, whereas, in third cycle, it was decreased to 69.53%.

3.9. Comparative performance of Fe_3O_4-CuO-AC with reported adsorbents

A comparison of the calculated maximum adsorption capacities (Qm) and removal efficiencies for BPB adsorption of other adsorbents in the literature are presented in Table 4.

The comparative study showsthat the method used in this study resulted in high adsorption capacity with time and dye removal efficiency for the Fe_3O_4-CuO-AC sample. Conclu-

Table 4 Comparison of adsorption capacity of BPB with other adsorbents.

Adsorbent	Removal efficiency (%)	Adsorption capacity (mg/g)	Optimum conditions	References
AgBr-ZnO nanocomposite	89.3	–	Dye concentration = 3 ppm, pH = 6.4, and adsorbent amount = 1.5 mg	Abdel-Khalek et al. (2018)
Activated carbon modified with CuS nanoparticle	–	106.4	pH = 7, adsorbent amount = 0.0091 g, 10 mg/L of BPB, and sonication time = 7 min	Mazaheri et al. (2016)
Fe_2O_3–ZnO–$ZnFe_2O_4$/carbon nanocomposite		90.91	Dye concentration = 15.5 mg/L, pH = 5.59, adsorbent amount = 0.005 g, and sonication time = 9 min	Mohammadzadeh et al. (2016)
α-chitin nanoparticles	–	22.72	Dye concentration = 15 mg/L, pH = 6, temperature = 15 °C, and adsorbent amount = 15 mg	Dhananasekaran et al. (2016)
CuO-NCP	32	–	7 ppm dyes, pH 5.9, catalyst dose of 0.2 g L^{-1}, and CuO loading of 4.9%	Nezamzadeh-Ejhieh and Zabihi-Mobarakeh (2014)
Activated carbon	–	51.21	10 mg L^{-1} dyes, pH = 1, and adsorbent dose = 1 g	Ghaedi et al. (2014)
Polymer-clay composite	–	10.78	Dye concentration = 50 mg/L, adsorbent dose 7.5 g/l, and Temp. 25 ± 2 °C	El-Zahhar et al. (2014)
Mesoporous hybrid gel	–	26.5 mmol kg^{-1}	Gel dose of 0.125 g, NaCl concentration is 0.1 M, and BPB concentration is 0.04 mM.	You et al. (2006)
Activated carbon-Fe3O4-CuO composite	97%	88.6 mmg/g	Dye concentration = 10 mg/L, adsorbent dose 0.1 g, pH = 5–6 and Temp. 25 ± 2 °C	The present study

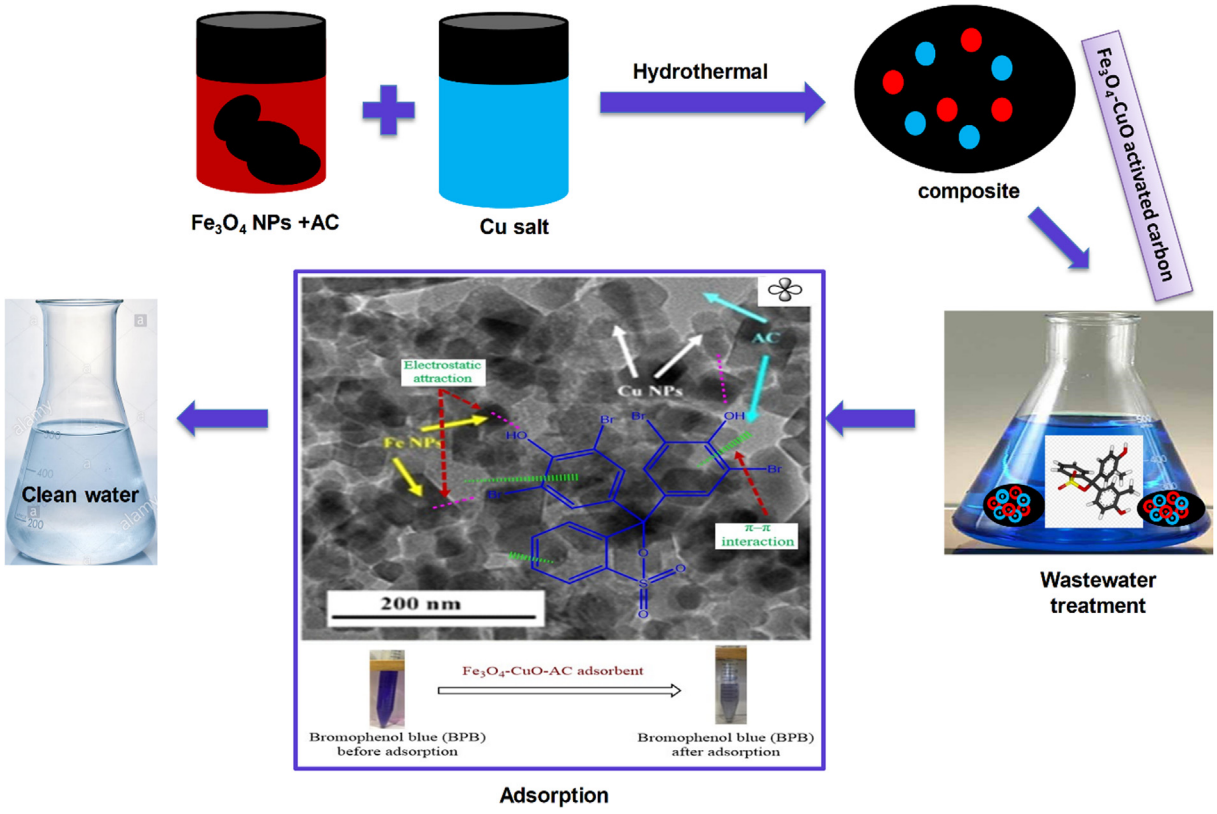

Fig. 11 Schematic diagram for composite synthesis and adsorption mechanism.

sively, the present method is preferred due to short time duration, less absorbent utilization and superior performance for dyes as compared to hitherto reported adsorbents. Fig. 11 represents the schematic diagram for composite synthesis and adsorption mechanism.

4. Conclusion

Iron and copper oxide nanoparticles loaded onto AC were synthesized and characterized by different physico-chemical methods. The composites were applied as adsorbent for the removal of five different dyes. The adsorption process fits a pseudo second-order model. The adsorption equilibrium time increased with an increase intemperature. It took about 70 min to reach the adsorption equilibrium at 15, 45 and 75 °C. The adsorption activation energy was found to be 2.583 $kJmol^{-1}$. The intraparticle diffusion of BPB into the Fe_3O_4-CuO-AC was found to be 16.494 $kJmol^{-1}$ and appeared to be a step of the overall adsorption process. Thermodynamic parameters ($\Delta S°$, $\Delta H°$ and $\Delta G°$) showed that the chemical adsorption process was Endothermic and spontaneous. Based on the presented results, the Fe_3O_4-CuO-AC composite can be regarded as a potential adsorbent for the removal of BPB dye from aqueous solutions which can help in controlling water pollution.

Declaration of Competing Interest

The authors declare that they have no known competing financial interests or personal relationships that could have appeared to influence the work reported in this paper.

Acknowledgements

We gratefully acknowledge the financial support by Albaha University (Project No. 1441/3) and are grateful to the Scientific Research Deanship and the Dean of the Faculty of Science at Albaha University for their encouragement in our research and for the use of the laboratory facility.

References

Abdel-Khalek, A.A., Mahmoud, S.A., Zaki, A.H., 2018. Visible light assisted photocatalytic degradation of crystal violet, bromophenol blue and eosin Y dyes using AgBr-ZnO nanocomposite. Environ. Nanotechnol. Monit. Manage. 9, 164–173.

Abdullah, A.Z., Salamatinia, B., Kamaruddin, A.H., 2009. Application of response surface methodology for the optimization of NaOH treatment on oil palm frond towards improvement in the sorption of heavy metals. Desalination 244 (1-3), 227–238.

Ahmadi, S., Chia, C.-H., Zakaria, S., Saeedfar, K., Asim, N., 2012. Synthesis of Fe3O4 nanocrystals using hydrothermal approach. J. Magn. Magn. Mater. 324 (24), 4147–4150.

Azari, A. et al, 2014. Nitrate removal from aqueous solution using carbon nanotubes magnetized by nano zero-valent iron. J. Mazandaran Univ. Med. Sci. (JMUMS) 23.

Azari, A. et al, 2017. Efficiency of magnitized graphene oxide nanoparticles in removal of 2, 4-dichlorophenol from aqueous solution. J. Mazandaran Univ. Med. Sci. 26 (144), 265–281.

Bhatnagar, A., 2007. Removal of bromophenols from water using industrial wastes as low cost adsorbents. J. Hazard. Mater. 139 (1), 93–102.

Bhattacharyya, K.G., Sharma, A., 2004. Azadirachta indica leaf powder as an effective biosorbent for dyes: a case study with aqueous Congo Red solutions. J. Environ. Manage. 71 (3), 217–229.

Cao, C.-Y., Zhang, T., Cong, Q., 2017. Adsorption of acid fuchsin onto the chitosan–montmorillonite composite. Mar. Georesour. Geotechnol. 35 (6), 799–805.

Daoud, M., Benturki, O., Girods, P., Donnot, A., Fontana, S., 2019. Adsorption ability of activated carbons from Phoenix dactylifera rachis and Ziziphus jujube stones for the removal of commercial dye and the treatment of dyestuff wastewater. Microchem. J. 148, 493–502.

Dashamiri, S., Ghaedi, M., Dashtian, K., Rahimi, M.R., Goudarzi, A., Jannesar, R., 2016. Ultrasonic enhancement of the simultaneous removal of quaternary toxic organic dyes by CuO nanoparticles loaded on activated carbon: central composite design, kinetic and isotherm study. Ultrason. Sonochem. 31, 546–557.

Dhananasekaran, S., Palanivel, R., Pappu, S., 2016. Adsorption of methylene blue, bromophenol blue, and coomassie brilliant blue by α-chitin nanoparticles. J. Adv. Res. 7 (1), 113–124.

El-Gamal, S.M.A., Amin, M.S., Ahmed, M.A., 2015. Removal of methyl orange and bromophenol blue dyes from aqueous solution using Sorel's cement nanoparticles. J. Environ. Chem. Eng. 3 (3), 1702–1712.

El-Zahhar, A.A., Awwad, N.S., El-Katori, E.E., 2014. Removal of bromophenol blue dye from industrial waste water by synthesizing polymer-clay composite. J. Mol. Liq. 199, 454–461.

Gao, Y., Yue, Q., Gao, B., Sun, Y., Wang, W., Li, Q., Wang, Y., 2013. Comparisons of porous, surface chemistry and adsorption properties of carbon derived from Enteromorpha prolifera activated by H4P2O7 and KOH. Chem. Eng. J. 232, 582–590.

Gautam, S., Agrawal, H., Thakur, M., Akbari, A., Sharda, H., Kaur, R., Amini, M., 2020. Metal oxides and metal organic frameworks for the photocatalytic degradation: a review. J. Environ. Chem. Eng. 8 (3), 103726. https://doi.org/10.1016/j.jece:2020.103726.

Ghaedi, M., Hekmati Jah, A., Khodadoust, S., Sahraei, R., Daneshfar, A., Mihandoost, A., Purkait, M.K., 2012. Cadmium telluride nanoparticles loaded on activated carbon as adsorbent for removal of sunset yellow. Spectrochim. Acta Part A Mol. Biomol. Spectrosc. 90, 22–27.

Ghaedi, M., Ghaedi, A.M., Negintaji, E., Ansari, A., Vafaei, A., Rajabi, M., 2014. Random forest model for removal of bromophenol blue using activated carbon obtained from Astragalus bisulcatus tree. J. Ind. Eng. Chem. 20 (4), 1793–1803.

Ghosh, U. et al, 2019. Adsorption behaviour of bromophenol blue from the aqueous solution on Labeo bata fish scale, a bio-waste material. Indian J. Chem. Technol. (IJCT) 26 (4), 321–329.

Hassan, M.S. et al, 2012. Smart copper oxide nanocrystals: synthesis, characterization, electrochemical and potent antibacterial activity. Colloids Surf., B 97, 201–206.

Ho, Y.-S., 2006. Second-order kinetic model for the sorption of cadmium onto tree fern: a comparison of linear and non-linear methods. Water Res. 40 (1), 119–125.

Hunger, K., 2003. Dyes, general survey. Industrial Dyes: Chemistry, Properties, Applications, Wiley Subscription Services, Inc., A Wiley Company, Frankfurt, p. 1–10.

Karami, A., Karimyan, K., Davoodi, R., Karimaei, M., Sharafie, K., Rahimi, S., Khosravi, T., Miri, M., Sharafi, H., Azari, A., 2017. Application of response surface methodology for statistical analysis, modeling, and optimization of malachite green removal from aqueous solutions by manganese-modified pumice adsorbent. dwt 89, 150–161. https://doi.org/10.5004/dwt.201710.5004/dwt.2017.21366.

Khan, M.A., Alam, M.M., Naushad, M.u., Alothman, Z.A., Kumar, M., Ahamad, T., 2015. Sol–gel assisted synthesis of porous nanocrystalline CoFe 2 O 4 composite and its application in the removal of brilliant blue-R from aqueous phase: an ecofriendly and economical approach. Chem. Eng. J. 279, 416–424.

Kim, S.-H., Choi, P.-P., 2017. Enhanced Congo red dye removal from aqueous solutions using iron nanoparticles: adsorption, kinetics, and equilibrium studies. Dalton Trans. 46 (44), 15470–15479.

Lagergren, S., 1898. Zur theorie der sogenannten adsorption geloster stoffe.

Lellis, B., Fávaro-Polonio, C.Z., Pamphile, J.A., Polonio, J.C., 2019. Effects of textile dyes on health and the environment and bioremediation potential of living organisms. Biotechnol. Res. Innovat. 3 (2), 275–290.

Li, S., Wang, D., Wu, X., Chen, Y., 2020. Recent advance on VOCs oxidation over layered double hydroxides derived mixed metal oxides. Chin. J. Catal. 41 (4), 550–560.

Liu, M., Chen, C., Hu, J., Wu, X., Wang, X., 2011. Synthesis of magnetite/graphene oxide composite and application for cobalt(II) removal. J. Phys. Chem. C 115 (51), 25234–25240.

Liu, W., Ge, H., Chen, X., Lu, X., Gu, Z., Li, J., Wang, J., 2019. Fish-scale-like intercalated metal oxide-based micromotors as efficient water remediation agents. ACS Appl. Mater. Interfaces 11 (17), 16164–16173.

Liu, J., Guo, D., Zhou, Y., Wu, Z., Li, W., Zhao, F., Zheng, X., 2011. Identification of ancient textiles from Yingpan, Xinjiang, by multiple analytical techniques. J. Archaeol. Sci. 38 (7), 1763–1770.

Malkoc, E., 2006. Ni(II) removal from aqueous solutions using cone biomass of Thuja orientalis. J. Hazard. Mater. 137 (2), 899–908.

Mazaheri, H., Ghaedi, M., Asfaram, A., Hajati, S., 2016. Performance of CuS nanoparticle loaded on activated carbon in the adsorption of methylene blue and bromophenol blue dyes in binary aqueous solutions: using ultrasound power and optimization by central composite design. J. Mol. Liq. 219, 667–676.

Moazzen, M., Mousavi Khaneghah, A., Shariatifar, N., Ahmadloo, M., Eş, I., Baghani, A.N., Yousefinejad, S., Alimohammadi, M., Azari, A., Dobaradaran, S., Rastkari, N., Nazmara, S., Delikhoon, M., Jahed Khaniki, GholamReza, 2019. Multi-walled carbon nanotubes modified with iron oxide and silver nanoparticles (MWCNT-Fe3O4/Ag) as a novel adsorbent for determining PAEs in carbonated soft drinks using magnetic SPE-GC/MS method. Arab. J. Chem. 12 (4), 476–488.

Mohammadzadeh, A., Ramezani, M., Ghaedi, A.M., 2016. Synthesis and characterization of Fe2O3–ZnO–ZnFe2O4/carbon nanocomposite and its application to removal of bromophenol blue dye using ultrasonic assisted method: optimization by response surface methodology and genetic algorithm. J. Taiwan Inst. Chem. Eng. 59, 275–284.

Naghan, D.J. et al, 2015. Parameters effecting on photocatalytic degradation of the phenol from aqueous solutions in the presence of ZnO nanocatalyst under irradiation of UV-C light. Bul. Chem. Commun. 47 (Specia), 14–18.

Nezamzadeh-Ejhieh, A., Zabihi-Mobarakeh, H., 2014. Heterogeneous photodecolorization of mixture of methylene blue and bromophenol blue using CuO-nano-clinoptilolite. J. Ind. Eng. Chem. 20 (4), 1421–1431.

Okoye, C., 2018. Adsorptive removal of bromophenol blue dye from aqueous solution using acid activated clay. Int. J. Sci. Res. Mana. 6 (03). https://doi.org/10.18535/ijsrm/v6i3.ce01.

Peternela, J., Silva, M.F.Vieira, M.F., Bergamasco, R., Vieira, A.M.S., 2018. Synthesis and impregnation of copper oxide nanoparticles on activated carbon through green synthesis for water pollutant removal. Mat. Res. 21 (1). https://doi.org/10.1590/1980-5373-mr-2016-0460.

Salari, M., Dehghani, M.H., Azari, A., Motevalli, M.D., Shabanloo, A., Ali, I., 2019. High performance removal of phenol from aqueous solution by magnetic chitosan based on response surface methodology and genetic algorithm. J. Mol. Liq. 285, 146–157.

Senthil Kumar, P., Varjani, S.J., Suganya, S., 2018. Treatment of dye wastewater using an ultrasonic aided nanoparticle stacked activated carbon: kinetic and isotherm modelling. Bioresour. Technol. 250, 716–722.

Shaheen, K. et al, 2020. Metal oxides nanomaterials for the photocatalytic mineralization of toxic water wastes under solar light illumination. J. Water Process Eng. 34, 101138.

Shu, J., Cheng, S., Xia, H., Zhang, L., Peng, J., Li, C., Zhang, S., 2017. Copper loaded on activated carbon as an efficient adsorbent for removal of methylene blue. RSC Adv. 7 (24), 14395–14405.

Sousa, V.S., Teixeira, M.R., 2020. Metal-based engineered nanoparticles in the drinking water treatment systems: a critical review. Sci. Total Environ. 707, 136077.

Tabassum, A. et al, 2015. Catalytic potential of gourd peel peroxidase for biodegradation of synthetic recalcitrant dyes fuchsin acid and crystal violet. J. Anim. Plant Sci 25 (3), 777–783.

Wang, T. et al, 2020. Roles of functional microbial flocculant in dyeing wastewater treatment: Bridging and adsorption. J. Hazard. Mater. 384, 121506.

Wang, Y., Shi, L.i., Gao, L., Wei, Q., Cui, L., Hu, L., Yan, L., Du, B., 2015. The removal of lead ions from aqueous solution by using magnetic hydroxypropyl chitosan/oxidized multiwalled carbon nanotubes composites. J. Colloid Interface Sci. 451, 7–14.

Wang, D.e., Xu, Y., Xiao, D., Qiao, Q., Yin, P., Yang, Z., Li, J., Winchester, W., Wang, Z., Hayat, T., 2019. Ultra-thin iron phosphate nanosheets for high efficient U(VI) adsorption. J. Hazard. Mater. 371, 83–93.

Wang, Y., Zhao, G., Zhang, G., Zhang, Y., Wang, H., Cao, W., Li, T., Wei, Q., 2020. An electrochemical aptasensor based on gold-modified MoS2/rGO nanocomposite and gold-palladium-modified Fe-MOFs for sensitive detection of lead ions. Sens. Actuators, B 319, 128313. https://doi.org/10.1016/j.snb.2020.128313.

Wu, J., Zhou, J., Zhang, S., Alsaedi, A., Hayat, T., Li, J., Song, Y., 2019. Efficient removal of metal contaminants by EDTA modified MOF from aqueous solutions. J. Colloid Interface Sci. 555, 403–412.

Xiang, Y. et al, 2019. Comparative study of three novel organo-clays modified with imidazolium-based gemini surfactant on adsorption for bromophenol blue. J. Mol. Liq. 286, 110928.

Xu, P.-F. et al, 2020. Microfluidic controllable synthesis of monodispersed sulfur nanoparticles with enhanced antibacterial activities. Chem. Eng. J. 398, 125293.

You, L., Wu, Z., Kim, T., Lee, K., 2006. Kinetics and thermodynamics of bromophenol blue adsorption by a mesoporous hybrid gel derived from tetraethoxysilane and bis(trimethoxysilyl)hexane. J. Colloid Interface Sci. 300 (2), 526–535.

Zhang, J., Huang, G.-Q., Liu, C., Zhang, R.-N., Chen, X.-X., Zhang, L., 2018. Synergistic effect of microbubbles and activated carbon on the ozonation treatment of synthetic dyeing wastewater. Sep. Purif. Technol. 201, 10–18.

Zhao, X., Urano, K., Ogasawara, S., 1989. Adsorption of polyethylene glycol from aqueous solution on montmorillonite clays. Colloid Polym. Sci 267 (10), 899–906.

Zheng, X., Yu, N., Wang, X., Wang, Y., Wang, L., Li, X., Hu, X., 2018. Adsorption properties of granular activated carbon-supported titanium dioxide particles for dyes and copper ions. Sci. Rep. 8 (1). https://doi.org/10.1038/s41598-018-24891-1.